Research article

Journal of RAMAN SPECTROSCOPY

Received: 30 July 2012 Revised: 7 November 2012 Accepted: 8 November 2012 Published online in Wiley Online Library: 10 January 2013

(wileyonlinelibrary.com) DOI 10.1002/jrs.4231

Raman spectroscopy as a probe of molecular order, orientation, and stacking of fluorinated copper-phthalocyanine ($F_{16}CuPc$) thin films

F. Cerdeira,[a,b] M. Garriga,[a] M. I. Alonso,[a]* J. O. Ossó,[c] F. Schreiber,[d] H. Dosch[e] and M. Cardona[f]

We report Raman scattering measurements on azimuthally ordered thin films of $F_{16}CuPc$, prepared by organic molecular beam deposition on A-plane sapphire substrates. The observed peak frequencies have been compared both to the results of a model calculation for the vibrational modes of the free molecule and to those reported by other authors in related materials. This analysis provides a plausible identification of the modes responsible for the strongest spectral features. Detailed evaluation of the spectra reveals that some observed modes, which correspond to vibrations of the macrocycle inner ring, largely retain the intramolecular character and their polarisation properties can be used to study the orientation and stacking configuration of the molecules. We provide structural parameters deduced either in molecular or crystal symmetry considering the simpler possibilities, i.e. a single column molecular stacking and a herringbone-like structure. The results suggest that the thicker and most ordered film is structurally close to the recently reported crystal organisation of bulk ribbon samples of this compound. The crystalline quality of the ordered films is mainly reflected in some other Raman peaks which are related to the motion of peripheral atoms and dominate the high wavenumber part of the spectra. These modes are affected by intermolecular interactions inducing Davydov splittings that are unequivocally identified by the observed Raman selection rules. The performed analysis also provides quantitative estimates of the degree of in-plane ordering. Copyright © 2013 John Wiley & Sons, Ltd.

Supporting information may be found in the online version of this article.

Keywords: Raman tensor; phthalocyanine; vibrational Davydov splitting; organic semiconductor

Introduction

The growth of thin films and multi-layer structures of organic semiconducting materials has shown great progress recently, mainly because of their interesting optoelectronic properties and the possibility to be used in certain types of applications.[1–4] In particular, high quality samples are now being produced by organic molecular beam deposition (OMBD).[1,5] Especially attractive are metallophthalocyanines ($X_{16}MPc$), where the combined action of end atoms (or groups of atoms), X, and the metal atom, M, determines the gap between the highest occupied molecular orbital (HOMO) and the lowest unoccupied one (LUMO), through hybridisation of the metal d-orbitals with the π-orbitals of the organic core.[6] This opens the possibility of changing the electronic properties with limited structural disturbances, thus making these materials good candidates for the eventual fabrication of multi-layer structures with a modulated energy gap and tailored conduction properties.[1,7,8] Specifically, $F_{16}CuPc$ has attracted strong interest as a candidate for air-stable n-conduction.[9] Raman scattering allows for an investigation of fundamental issues affecting the optoelectronic and charge transport properties: On the one hand, film nanostructure issues such as ordering and molecular packing, and on the other, experimental vibrational properties which are important to refine theories where precise knowledge of vibration frequencies and atomic displacements are needed to model charge transport at molecular level.[10–12]

The crystalline structures of these $F_{16}CuPc$ films are not precisely known. Like most metallophthalocyanines with not too big central ion, the free $F_{16}CuPc$ ($C_{32}F_{16}N_8Cu$) molecule depicted in Fig. 1(a) is planar and has D_{4h} symmetry. This kind of molecules usually crystallise in various polymorphic forms of similar structures that consist of molecular columns with a herringbone-type arrangement between the columns. For example, for the homologous molecule $H_{16}C_{32}N_8Cu$ (hydrogenated CuPc) up to 10 polymorphs have been reported[13] although the most stable bulk phase is the β-CuPc.[14] This is a monoclinic crystal structure (space group C_{2h}^5) with two molecules per primitive cell (PC) which are equivalent with respect to a reflection plane perpendicular to the *b*-axis. These molecules

* *Correspondence to: M. I. Alonso, ICMAB-CSIC, Campus de la UAB, E-08191 Bellaterra, Spain. E-mail: isabel.alonso@icmab.es*

a *Institut de Ciència de Materials de Barcelona, ICMAB-CSIC, Campus de la UAB, E-08193 Bellaterra, Spain*

b *Instituto de Física "Gleb Wataghin", UNICAMP, 13083-859 Campinas, S.P., Brazil*

c *MATGAS Research Center, Campus de la UAB, E-08193 Bellaterra, Spain*

d *Institut für Angewandte Physik, Universität Tübingen, Auf der Morgenstelle 10, 72076 Tübingen, Germany*

e *Deutsches Elektronen Synchrotron (DESY), Notkestr. 85, D-22607 Hamburg, Germany*

f *Max-Planck-Institut für Festkörperforschung, Heisenbergstr. 1, D-70569 Stuttgart, Germany*

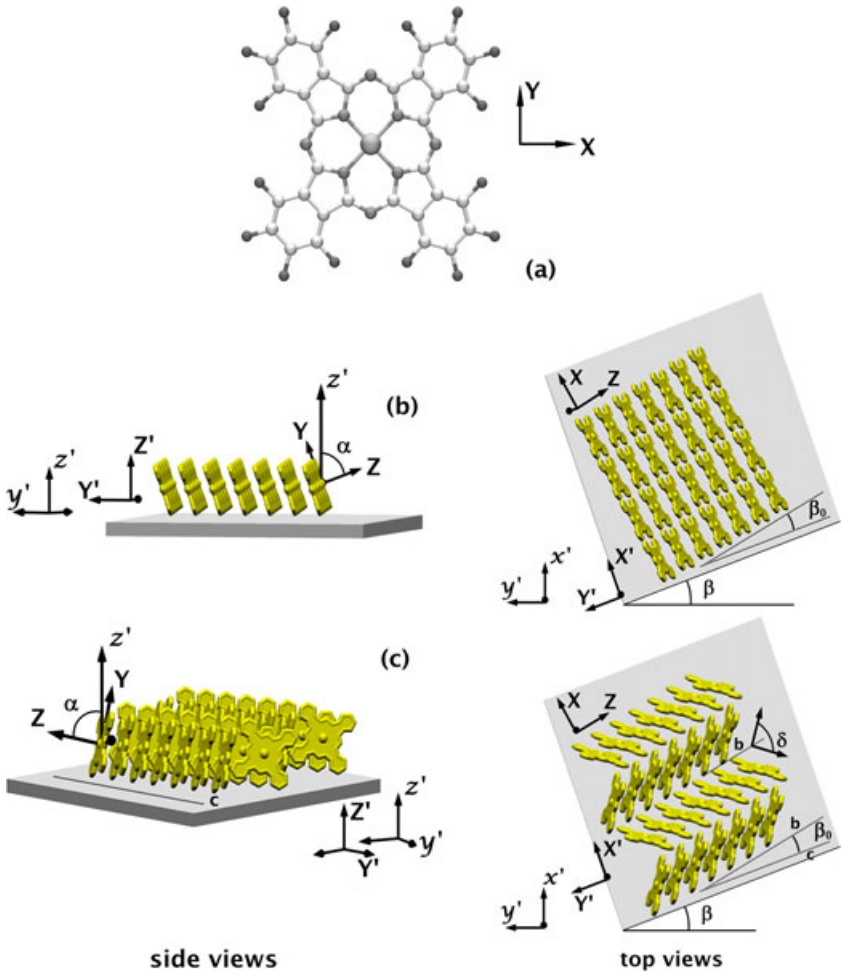

Figure 1. (a) Chemical structure of F_{16}CuPc, X and Y identify the axes set used for the Raman tensors and intensity calculations. (b) Type I and (c) Type II stacking of molecules in a F_{16}CuPc thin film on a sapphire substrate. *x′y′z′* are the laboratory axes, *X′Y′Z′* define the substrate orientation and *XYZ* describe either the molecular (b) or the monoclinic crystal (c) orientation. Also shown are the angles used in Eqn (6) and Table 2.

define a herringbone with an apical angle δ as displayed in Fig. 1(c), and the monoclinic *b*-axis lies in the direction of the bisectrix of the two molecular plane normals. Many of the polymorphs just differ in the value of this angle which for the β-CuPc is around 90°. Other common phases are the γ-CuPc where $\delta \sim 120°$ and the metastable phase α-CuPc which can be found in thin films[13] is also monoclinic and consists of stacked molecules with a tilt angle of about 25° from the *b*-axis but not forming a herringbone. Such a case with molecules stacked along the *b*-axis is represented in Fig. 1(b). Some structural phases of fluorinated CuPc have been reported. In ribbons of F_{16}CuPc, a structure with somewhat different lattice parameters but similar to β-CuPc was proposed.[15] Recently, another bulk structure was refined and reported to be triclinic,[16] however with two crystallographically independent molecules per PC forming a herringbone with $\delta = 146°$. In thin films with thicknesses beyond two monolayers, a monoclinic structure similar to β-CuPc[17] was proposed and the herringbone angle estimated to be $\delta \sim 90°$. Below two monolayers, the structure was more similar to single molecular stacking like in the α-CuPc phase.[17] Based on the available X-ray and spectroscopic investigations, the structural phases of the present ordered films[18–22] are consistent with a monoclinic structure with C_{2h} point group symmetry. Although the question of solid-state packing in the ordered films cannot be solved with one single technique, Raman scattering gives some interesting insights into the problem. Another question is whether there is more than one molecule per PC. In such case, the internal vibrations of the symmetry equivalent molecules may couple giving rise to a correlation field effect or Davydov splitting of the modes. As will be explained below, this effect can be detected by analysis of the Raman polarisation of the modes, which is easier using oriented single crystal samples. In a few single crystals of related materials, the presence of Davydov doublets of some internal modes was previously identified: In sexithiophene (6T) by applying high hydrostatic pressure[23,24] and in the perylene derivative PTCDA using the Raman polarisation dependence.[25] The effect was also detected in not quite ordered films of pentacene[26] by depolarisation variations in the spectra.

The vibrational spectra of phthalocyanines have been investigated in many previous works, see for example Refs. 27–33. Basova *et al.*[34] reported recently a complete experimental study including data on a single crystal of β-CuPc and assigned most observed Raman and infrared modes based on the molecular D_{4h} symmetry. Unequivocal assignments of the Raman spectrum of the material were facilitated by having oriented single crystals and a reliable calculation of the vibrational spectrum. No Davydov splittings due to influence of the crystalline environment were detected in their experiments. Incidentally, these authors[34] discussed contradictory assignments found in former

literature of Raman spectra of metallophthalocyanines; therefore, we refer to their work for discussion of earlier literature. In films of the fluorinated compound $F_{16}CuPc$, a recent paper[11] reported Raman spectra and discussed them likewise based on the molecular D_{4h} symmetry. The authors looked for hints to Davydov doublets by measuring the depolarisation ratio of the Raman spectra, but contrary to the case of pentacene[26], they did not detect any depolarisation variations in the spectra of azimuthally unordered $F_{16}CuPc$.

In this work, we study $F_{16}CuPc$ films grown on A-plane $(11\bar{2}0)$ sapphire substrates under different growth conditions. We concentrate on films showing evidence of both in- and out-of-plane order. In this orientation, the sapphire *c*-axis lies on the substrate surface; preliminary optical experiments, namely Raman scattering and spectroscopic ellipsometry,[18,19] together with non-contact atomic force microscopy and X-ray diffraction experiments[20] revealed that in-plane order is induced by the regular step pattern on the surface of the substrate.[22,21] In what follows, we discuss in detail the characterisation of several $F_{16}CuPc$ films by Raman scattering. With plausible assignments of the symmetry of some features in the Raman spectra, aided by a model calculation of the azimuthal dependence of the Raman intensity of molecular vibrational modes, it is possible to obtain quantitative values for parameters such as the angles between the plane of the molecule and that of the film and between two symmetry-equivalent molecules, as well as the orientation of the molecular and/or crystalline symmetry axis relative to the optical *c*-axis of the substrate. We analyse the spectra both using the molecular D_{4h} as well as the crystalline C_{2h} symmetry and discuss detected Davydov splitted components in some modes. In absence of data from single crystalline material of the compound, the data on the best ordered films provide an improved reference for the Raman spectrum of $F_{16}CuPc$ crystals.

Experiments and methods

All investigated films were deposited under ultra high vacuum conditions by OMBD. The $F_{16}CuPc$ powder was purchased from Aldrich Chemical Co. and purified twice by gradient sublimation prior to evaporation from a custom-built Knudsen cell. A quartz crystal device placed close to the substrate monitored film thickness and deposition rates. Films of different thicknesses were deposited at substrate temperatures (T_{sub}) varying between $-150\,^{\circ}C$ and $250\,^{\circ}C$. Details of sample preparation and structural studies are gathered in Ref. 22. As a consequence of a 0.57 degrees miscut, annealed sapphire A-plane substrates consist of a stepped surface with terrace widths of approximately 130 nm and 1.8 nm step heights with step edges being oriented almost perpendicular to the sapphire *c*-axis. Ordered $F_{16}CuPc$ films studied here display an in-plane anisotropy which has been related to the stepped substrate surface.[22,21] A list of samples used in our Raman experiments is given in Table 1.

Raman measurements were made at room temperature using a power density $\sim 1.5 \times 10^4$ W/cm^2 (~ 0.15 mW/μm^2) of the 514.5 nm line of an argon-ion laser as exciting radiation. Scattered light was analysed with a Jobin Yvon T-4000 XY triple spectrometer equipped with a multichannel charge-coupled device detector. An optical microscope with a ×50 objective was used to focus the laser beam on the sample and collect the scattered light. The laser light spot on the sample was between 1 and 2 μm in diameter. The spectral resolution was ~ 2 cm^{-1}.

Table 1. Relevant structural parameters of the samples, grown on annealed A-plane sapphire substrates, used in our experiment. The last column lists the order parameter obtained via Eqn (9), using the 733 cm^{-1} line of the Raman spectrum of each sample

Designation	Substrate temperature (°C)	Thickness (nm)	Order parameter v
S1	49	20	0.90 ± 0.04
S2	230	5	0.3 ± 0.2
S3	230	12	0.93 ± 0.03
S4	230	20	0.96 ± 0.02
S5	230	50	1.00 ± 0.01

All measurements were performed in the backscattering configuration and in the 150 to 1600 cm^{-1} wavenumber interval. Spectra with parallel (P) and crossed (C) polarisations were recorded. These are designated, respectively, by: $\bar{z}'(x',x')z'$ and $\bar{z}'(x',y')z'$, where z' is the laboratory axis perpendicular to the film surface (the $x'y'$-plane). The scattered intensity depends on the orientation of these laboratory axes to the principal symmetry axes of either the molecule or the crystal, which are designated by *X*, *Y*, and *Z*, with *Z* parallel to the C_4 symmetry axis of the $F_{16}CuPc$ molecule or to the C_2 axis of the corresponding monoclinic crystal. Our choice of *X* and *Y* axes in the plane of the molecule, among the two possibilities for a tetragonal molecule, is indicated in Fig. 1 (a). Similarly, the relative orientation of the sapphire substrate will be given by the coordinate system axes *X*′, *Y*′, and *Z*′, where the crystallographic sapphire *c*-axis coincides with *Y*′ and *Z*′ is perpendicular to the substrate surface. This gives the *X*′-axis parallel to film surface. In all experiments, the incident polarisation was kept constant along the x' axis. For measurements of the angular dependence of the intensity of the Raman peaks, the sample was mounted on a goniometer, which was manually rotated in different angular increments (mostly of 5° or 10°), around the z' axis. Care was taken in centring the sample so that upon rotation, the beam remained within a narrow region around the initial spot. We estimate that all our angular measurements were performed within a circle with a diameter not larger than ten times the size of the laser spot (i.e. about 15 μm). For these experiments, the rotation angle, β, is defined as that between the laboratory x'-axis and the *X*′-axis of the sapphire A-plane substrates. The value of β is determined by monitoring the intensity of the A_{1g} peak of sapphire, located at 644 cm^{-1}, in both parallel and crossed polarisations. Because this is an A_{1g} vibration with only $Z'Z'$ component (a_s 0),[35] its intensity depends on β through:

$$I\left(x',x'\right) = b_s^2 \sin^4\beta, \qquad I\left(x',y'\right) = \frac{b_s^2}{4}\sin^2 2\beta, \tag{1}$$

where b_s is an amplitude parameter, obtained in arbitrary units by fitting the Raman intensity of this peak *versus* β with Eqn (1). This expression was tested by measuring the Raman spectrum of a bare substrate and found to describe the observed angular dependence of intensities to within a 1% accuracy. These spectra were also used to identify and subtract from the spectra of the samples those peaks originated at the substrate. The orientation of the molecules (or crystallites where applicable) on the substrate is defined by two angles: α, the angle between the *Z* and z' axes, and β_0, the angle between the *X* and *X*′ axes

(assumed to be on the $x'y'$-plane). In Fig. 1, we represent the chemical structure of the material under study and illustrate the definition of angles α and β_0. The latter accounts for small alignment differences of the X and X' axes which were also observed by ellipsometry.[19] The angles α and β are actually Eulerian angles which describe the relationship between laboratory axes and symmetry axes in each case. We use active rotations and the notation β, α, and γ for the first, second, and third rotations, respectively.

Assignment of the observed modes was done by comparison to the closest references of CuPc single crystal[34] and F_{16}CuPc films on SiO_2[11] and also taking into account the results of a model calculation for the normal modes of the free molecule. We used the B3LYP/6-31 G approximation in Gaussian98.[36] Approximate atom coordinates were obtained from existing crystal structure data[14,37] and optimised within Gaussian98 before calculating the normal modes. This calculation serves as an auxiliary tool to assign the modes paying special attention to the normal mode atomic displacements and the mode symmetries, and less to the exact frequencies. The correspondence between calculated and experimental Raman frequencies is detailed below. No scaling factor was applied to the calculations. A linear best fit of the corresponding frequencies gives a zero intercept and an almost unity scaling factor: $\omega_{calc} = (0.998 \pm 0.003)\omega_{expt}$. This average agreement results from both positive and negative deviations $\omega_{calc} - \omega_{expt}$, the largest being found at the highest frequencies, above 1400 cm^{-1}.

Symmetry considerations

The free F_{16}CuPc ($C_{32}F_{16}N_8Cu$) molecule is planar and contains 57 atoms.[27,29] The central Cu atom site has the full molecular D_{4h} symmetry, whereas the other atomic site symmetries are subgroups of it as follows: $57 = 1Cu(D_{4h}) + 4N_1(C_{2v}) + 4N_2(C_{2v}) + 4 \times 8C(C_s) + 2 \times 8F(C_s)$. The isolated molecule has $3 \times 57 - 6 = 165$ normal modes of vibration (intramolecular vibrations) which are distributed among the representations of the D_{4h} point group according to:[27,32]

$$\begin{aligned}\Gamma(\text{vib}) = {} & 14\ A_{1g} + 13\ A_{2g} + 14\ B_{1g} + 14\ B_{2g} + 13\ E_g \\ & + 6\ A_{1u} + 8\ A_{2u} + 7\ B_{1u} + 7\ B_{2u} + 28\ E_u,\end{aligned} \quad (2)$$

of which only the in-plane A_{1g}, B_{1g}, B_{2g} and out-of-plane E_g modes are Raman active. Note that E representations are bidimensional, i.e. give rise to doubly degenerated vibration modes. The relationship between site symmetries and vibration modes of Eqn (2) is detailed as Supporting Information in Table S1. The Raman tensors of the active modes have the form:[32]

$$A_{1g}: \begin{pmatrix} a_o & 0 & 0 \\ 0 & a_o & 0 \\ 0 & 0 & b_o \end{pmatrix}, B_{1g}: \begin{pmatrix} c_o & 0 & 0 \\ 0 & -c_o & 0 \\ 0 & 0 & 0 \end{pmatrix}, B_{2g}: \begin{pmatrix} 0 & d_o & 0 \\ d_o & 0 & 0 \\ 0 & 0 & 0 \end{pmatrix}$$
$$E_g: \begin{pmatrix} 0 & 0 & 0 \\ 0 & 0 & e_o \\ 0 & e_o & 0 \end{pmatrix}, \text{ and } \begin{pmatrix} 0 & 0 & e_o \\ 0 & 0 & 0 \\ e_o & 0 & 0 \end{pmatrix}. \quad (3)$$

These tensors are referred to the principal molecular axes X, Y, and Z already defined.

Since we are concerned with crystalline films, it is necessary to correlate the molecular point group to the site group and factor group to obtain the selection rules in the crystalline molecular structures.[38] The two common forms of molecular stacking which are possible in the ordered films are represented in Fig. 1. In one of them, (similar to α-CuPc or type I stacking), molecules are stacked parallel to one another [Fig. 1(b)]. The alternative (type II stacking) is the formation of crystallites with a herringbone molecular stacking involving two molecules per PC [Fig. 1(c)]. Regardless of the exact stacking, the factor group of the crystal is expected to be monoclinic and centrosymmetric, that is, C_{2h}. The number of internal modes will be a multiple of 165. Compared to the intramolecular modes, these internal modes can be affected by two types of changes. First, the frequency of a given mode may be shifted from the free molecule value while the reduced symmetry of the crystalline arrangement may give rise to splittings in degenerate molecular modes (E_g). The corresponding Raman selection rules become those given by the Raman tensors of the point group of the crystal (C_{2h}), rather than those of the free molecule (D_{4h}). The second effect is the Davydov splitting of non-degenerate molecular modes into multiplets if there is more than one molecule per PC. In the present case of two molecules per PC, the number of internal modes is 330. In addition, there are nine external modes originating in rigid vibrations or rotations of the molecules within a PC. The modes are distributed among the irreducible representations of the factor group according to:[28,31]

$$\begin{aligned}\Gamma(\text{external}) &= 3A_g + 3B_g + 2A_u + B_u \\ \Gamma(\text{internal}) &= 81A_g + 81B_g + 84A_u + 84B_u\end{aligned} \quad (4)$$

The mode distributions are obtained considering the molecular site symmetry which is C_i. For the internal modes, the result of the correlation method[39] is given as Supporting Information in Table S2. The symmetries of the external modes considering two molecules at C_i sites are detailed in Table S3. The Raman active A_g and B_g modes have Raman tensors of the general form:

$$A_g: \begin{pmatrix} a & d & 0 \\ d & b & 0 \\ 0 & 0 & c \end{pmatrix}, \qquad B_g: \begin{pmatrix} 0 & 0 & e \\ 0 & 0 & f \\ e & f & 0 \end{pmatrix}. \quad (5)$$

In the above expressions, a set of axes (X, Y, and Z) is chosen such that the crystallographic one (C_2 or b-axis) is along the Z direction and the XY-plane is perpendicular to it.

From all the vibration modes, the external ones are clearly characteristic of the crystalline lattice and can be used as a fingerprint of the crystal structure.[40,41] Because the intermolecular forces are usually much weaker than the covalent intramolecular ones and the involved masses are larger, these lattice modes normally appear at the low wavenumber region of 10–150 cm^{-1}.[41] With our experimental conditions, we were limited to the range above 150 cm^{-1}, and hence we discuss spectral features which will correspond to internal molecular vibrations. Also, due to the relatively weak intermolecular interaction, in molecular crystals, internal vibrations differ little from the intramolecular modes, and their selection rules can be considered to obey Eqn (3) if we take into account the 'fixed' orientation of the molecules in the crystal in a similar way as the oriented gas model.[40,42] In this way, the internal modes give information about the orientation of the molecules in relation to the laboratory axes. If we analyse the selection rules using Eqn (5), the angular dependence of the Raman intensities will be determined by the orientation of the crystal axes with respect to the laboratory ones. In both cases, we can relate the angular variation of the Raman

intensities to structural parameters. Specifically, for an ordered film, the angular variation of the Raman intensities depend on the angle (α) between the Z and z'-axes and that between the X and x' ones, assuming that the X-axis is contained in the plane of the film. The latter can be easily measured in relation to the direction of the c-axis of the sapphire substrate. Hence, for a given orientation of the sample, measured through the previously defined angle β, the Raman intensities depend on the angles α and β_0. Here, β_0 is the angle between the X-axis of the molecule or crystallite and that of the substrate or, equivalently, between the projection of the symmetry axis of the molecule or crystallite on the plane of the film and the c-axis of the sapphire substrate. The equations describing the way in which the intensity of modes of different symmetry (molecular or crystalline) depend on these angles are collected in Table 2.

Results and discussion

Raman spectroscopy as a tool can be efficiently used to explore the structure of not perfectly ordered crystalline materials. Qualitative differences in the Raman spectra of different films of the same compound can be related to structural diversity. In general, crystalline order (or the lack of it) is evidenced by the variations observed when the sample is rotated around the z'-axis. This feature is illustrated in Fig. 2, where spectra for two films of different thickness grown at the same substrate temperature (230 °C) are compared for both C and P configurations for three different values of the azimuthal angle β. For a given sample orientation, there are large differences between spectra taken with C and P configurations, that is, the depolarisation ratio is not the same for all modes. However, for a given polarisation, only the thicker film shows dramatic changes in the intensities of the Raman peaks as the azimuthal angle β varies. This is because strong in-plane order is only present in the thicker of the two films. We shall pursue this question quantitatively later.

Films deposited at lower substrate temperature also show evidence of order. However, we notice that some qualitative changes in the Raman spectra are observed among samples grown at different temperatures. This is shown as Supporting Information in Fig. S1, where the upper part (a) displays spectra of films of roughly equal thicknesses, but grown at different substrate temperature: 230 °C (bottom curve) and 49 °C (top curve), respectively. The bottom part [Fig. S1(b)] compares the spectra of samples of different thickness grown at the same substrate temperature (230 °C). All samples in Fig. S1 were oriented so that their azimuthal angle, β, is approximately zero. Important qualitative differences are found only between the spectra of samples grown at different substrate temperatures, while those of samples grown at the same temperature are very similar. Sample S1, grown at the lower temperature (49 °C), shows additional peaks in the low wavenumber range ($\omega < 1250\ cm^{-1}$) as well as broader peaks in the high wavenumber range. Table S4 (Supporting Information) lists peak positions and intensities in all spectra of representative samples, normalised taking as reference a strong peak which appears at $\sim$ 733 cm^{-1} in all spectra. The specific differences involved in the crystal structures of samples grown at different temperatures, as inferred from the Raman spectra, shall be discussed in the context of the angular dependence of Raman intensities. Generally, both structural and optical studies seem to indicate that the deposition temperature affects the internal crystal structure of the crystallites composing the film, whereas film thickness mainly, but not exclusively, affects the in-plane ordering of these crystallites. For a quantitative discussion of these aspects, we must consider the expected polarisation dependence of the Raman spectra as well as the assignments of the observed peaks. In the following, we describe these two parts of the problem.

Table 2. Angular dependence of Raman intensities. Here $x'y'z'$ are laboratory axes (Fig. 1), with z' normal to the plane of the film and x' parallel to the polarisation of the incoming laser light. P- and C-configurations are, respectively $\bar{z}'(x'x')z'$ and $\bar{z}'(x'y')z'$. Axes XYZ are the axes of the molecule (crystal) defined in Fig. 1 with Z along the C_4 (C_2) symmetry axis. Angles α and $\phi = \beta - \beta_0$ are, respectively, those between z' and Z and x' and X. We assume that X is contained in the plane of the film ($x'y'$)

(a) Monoclinic crystal

Mode	$I(x'x')$	$I(x'y')$
A_g	$(A\cos^2\phi + B - D\sin 2\phi)^2$	$\left(\frac{A}{2}\sin 2\phi + D\cos 2\phi\right)^2$
B_g	$4E^2\sin^2\phi\sin^2\alpha$	$F^2\sin^2\alpha$
$A = a - B$		
$B = b\cos^2\alpha + c\sin^2\alpha$		
$D = d\cos\alpha$		
$E = e\cos\phi - f\cos\alpha\sin\phi$		
$F = e\cos 2\phi - f\cos\alpha\sin 2\phi$		

(b) Molecular modes

Mode	$I(x'x')$	$I(x'y')$
A_{1g}	$(A\cos^2\phi + B)^2$	$\frac{A^2}{4}\sin^2 2\phi$
B_{1g}	$(C\cos^2\phi - c_0\cos^2\alpha)^2$	$\frac{C^2}{4}\sin^2 2\phi$
B_{2g}	$d_0^2\cos^2\alpha\sin^2 2\phi$	$d_0^2\cos^2\alpha\cos^2 2\phi$
E_g	$4e_0^2\sin^2\alpha\sin^2\phi\ (\sin^2\alpha\cos^2\phi + \cos^2\alpha)$	$e_0^2\sin^2\alpha\ (\sin^2\alpha\cos^2 2\phi + \cos^2\alpha)$
$A = (a_0 - b_0)\sin^2\alpha$		
$B = a_0\cos^2\alpha + b_0\sin^2\alpha$		
$C = c_0\ (1 + \cos^2\alpha)$		

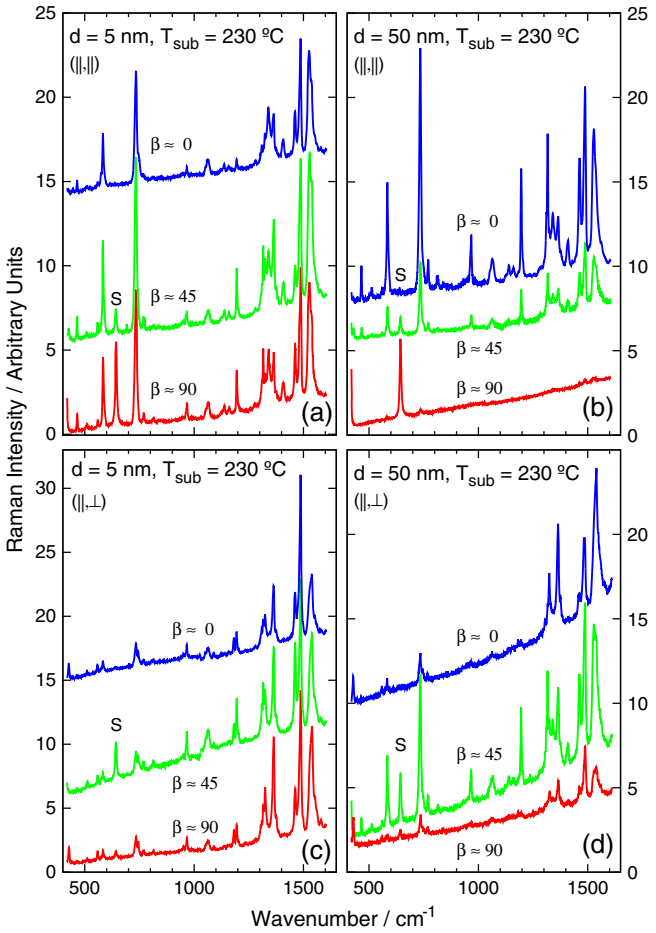

Figure 2. Comparison between the spectra of two samples of different thickness grown at 230 °C. This comparison is made for three different in-plane angular orientations ($\beta \approx$ 0, 45, and 90 deg, respectively) and both in P and C polarisations. Both samples contain modes with different depolarisation ratios, but only the spectra of the thicker film show variations depending on the azimuthal rotation around the surface normal. The latter are indicative of in-plane order. The peaks labeled S are due to the substrate.

Mode assignment and Davydov splittings

In order to derive structural parameters from the measured angular dependence of Raman intensities, a crucial question is whether the spectral feature being studied retains its intramolecular character or not. Different vibration modes can differ in their degree of localisation and probe several length scales in the crystal. Rather unperturbed modes are more likely to give rise to isolated peaks in the Raman spectrum, exhibiting either weak or no internal structure (for example, they are not part of a Davydov doublet). Hence, the presence or absence of Davydov splittings should be a good test to distinguish between modes that are affected by the intermolecular interactions and modes that remain essentially unaffected.

In Table S4 (Supporting Information), we list the experimental wavenumbers in β-CuPc and their symmetry assignments from Basova *et al.*[34] and the same information for F_{16}CuPc both from Wu *et al.*[11] and from our experiments. For comparison, we provide calculated frequencies of molecular modes and brief descriptions of the main atomic displacements involved in A_{1g} modes, which are characteristic of the different spectral ranges. We also provide relative intensities of the Raman peaks observed for our samples. The correspondences established in Table S4 try to match both similar frequencies and mode symmetries among the different works. There is good agreement between the F_{16}CuPc frequencies except for a few cases and also fair parallelism with the β-CuPc case, although in general peaks appear shifted *versus* the nonfluorinated parent compound, in some cases by as much as $\sim$ 50 cm^{-1}, as is the case for the A_{1g} peak at 733 cm^{-1} which is one of the strongest features. All calculated A_{1g} molecular modes can be related to observed features in the Raman spectra, although often two experimental peaks must be assigned to the same molecular vibration. This is another difference with respect to the cited literature, namely, the observation of a wealth of additional peaks. We interpret this fact as a sign of Davydov doublets and the corresponding structures are highlighted by shading in Table S4. The clearest examples of these splittings are found in the phonon wavenumber regions between 900 cm^{-1} and 980 cm^{-1} and between 1300 cm^{-1} and 1340 cm^{-1}, displayed in Fig. 3. An experimental observation is that the spectral region above 900 cm^{-1} shows closely spaced structures which are good candidates for assignment to Davydov doublets, whereas the region below 900 cm^{-1} is composed mainly of narrow, isolated structures that appear at the same wavenumber in all samples, regardless of growth conditions. The calculated normal mode amplitudes corresponding to different strong spectral features are shown in Fig. S2 (Supporting Information), together with our assignment to singlets and *doublets*. Comparing both types of structures, it is apparent that the former involve distortions of the internal macrocycle whereas the latter predominantly contain motions of the more peripheral atoms.

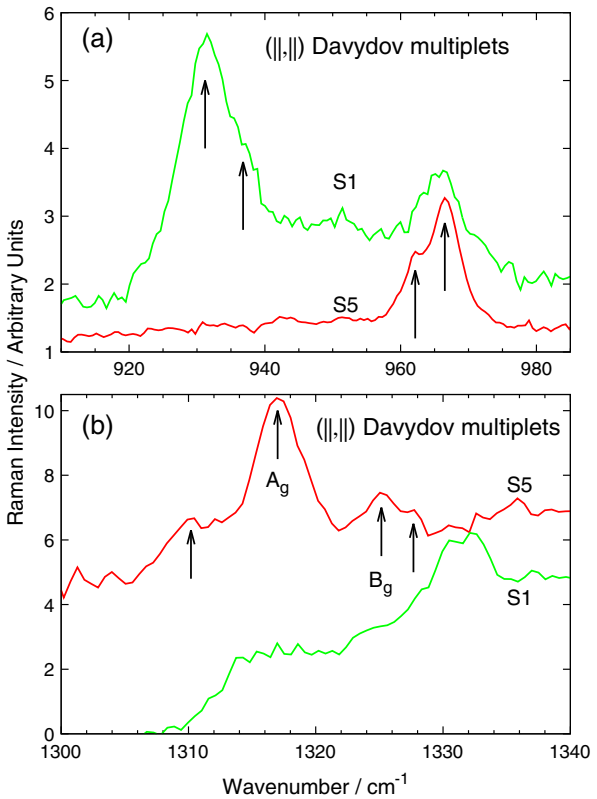

Figure 3. Groups of peaks in spectral regions where samples grown at different temperatures display not coincident spectra. Possible Davydov doublets are indicated in this example for samples S1 and S5.

The above discussion assigns most strong spectral features to molecular vibrations of A_{1g} symmetry. We also see some other in-plane modes such as B_{1g} and B_{2g} and no out-of-plane E modes, which are expected to be very weak since E modes mainly involve bond bendings. As in CuPc[34], it is also possible that some peaks are due to A_{2g} silent modes whose Raman intensity may be activated by distortion of the molecule from the planar configuration. The predominant observation of totally symmetric A_{1g} modes is common in the literature, especially if the Raman experiment is resonantly excited. As an example, see the works on PTCDA[43] and DIP,[44] where all the spectral features are derived from A_g molecular modes. This is attributed to the proximity between the laser lines used and the HOMO-LUMO optical transitions which produce symmetric charge displacements and only couple to fully symmetric vibrations. Basova *et al.*[34] used mainly non resonant excitations with laser lines at 488 nm (2.54 eV) and 532 nm (2.33 eV). In our measurements with the 514 nm line (2.41 eV), we are in similar conditions. In contrast, Wu *et al.*[11] used resonant excitation with the 633 nm laser (1.96 eV) to enhance their signals which using 532 nm excitation were rather weak. In fact, some A_{1g} lines were shown to have the largest resonant enhancements, but in general, the same lines could be observed irrespective of the excitation wavelength.

Figure 3 shows the most likely candidates for assignment to Davydov doublets in the Raman spectra of samples S1 and S5. In the wavenumber region around 930 cm^{-1}, both spectra show distinct, strong structures centered at frequencies of 931 cm^{-1} (S1) and 966 cm^{-1} (S5), respectively. The 966 cm^{-1} band in the lower curve is clearly split into a doublet, with $\Delta\omega \approx 4.5$ cm^{-1}, whereas the 931 cm^{-1} band of the upper spectrum is asymmetric towards higher energy, pointing to a barely resolved doublet. However, the angular behaviour of the intensities of these doublets cannot be measured accurately in order to establish their $A_g - B_g$ character unequivocally. Hence, it is difficult to assert that this is really an example of Davydov doublets. Another possible splitting is found at higher frequencies in the spectrum of sample S5 (Fig. 3). Here, the angular dependence of the intensities of two members of this multiplet (arrows) can be measured and is consistent with the $A_g - B_g$ symmetry of a Davydov doublet. This shall be discussed in more detail in the following section.

Angular dependence of the Raman intensities

In samples showing a high degree of order, the intensities of all strong spectral lines in the parallel polarisation configuration follow a periodicity of 180 degrees as a function of β. Peak intensities are highest when the incoming light is polarised *perpendicular* to the sapphire c-axis ($\beta \approx 0$ deg) and lowest when it is *parallel* ($\beta \approx 90°$) [Fig. 2(b)]. For crossed polarisations, a distinction must be made between the relatively isolated structures at frequencies below 900 cm^{-1} and the doublets above this wavenumber. For the former, the periodicity is 90°, with maximum intensities for β approximately equal to 45 degrees in well-ordered samples [see Fig. 2(d)]. Some of the components of the higher wavenumber clusters, however, do not follow this angular dependence, as can be seen also in Fig. 2(d). Thus, the two parts of the spectrum are expected to give different information and must be discussed separately according to the diverse observations.

We start with the angular dependence of the intensities of most peaks, in particular those at the lower wavenumber part of the spectrum. This dependence is well described by:

$$\begin{aligned} I(x',x') &= \left(A\cos^2(\beta-\beta_0)+B\right)^2 \\ I(x',y') &= A'\sin^2 2(\beta-\beta_0), \end{aligned} \tag{6}$$

where A, A', B, and β_0 are treated as adjustable parameters. This dependence is characteristic of fully symmetric modes of either molecular (A_{1g}) or crystalline (A_g) origin. In the latter case, the crystallographic b-axis must be contained in the plane of the film because, in this case, the parameter D is zero for A_g modes (see Table 2). Thus, the angular dependence is the same in both cases, but the physical interpretation given to the ratio between the fit parameters A and B is different. If a vibration mode is relatively independent of intermolecular interaction and thus it is localised at intramolecular length scale, the ratio A/B can be related to molecular structural parameters. Assuming that the angle between the molecular and film planes (α) is the same for all molecules (most simply considering the type I stacking), the relationship is given through (Table 2):

$$\tan^2(\alpha) = \frac{A/B}{1-\varepsilon(A/B)}, \tag{7}$$

where $\varepsilon = b_0/a_0$, is the ratio between the out-of-plane and in-plane components of the molecular Raman tensor for an A_{1g} mode. Since the molecule is planar, this ratio (ε) will be small, and in fact some authors[32] take it as equal to zero for practical purposes. If this ratio were small for a significant number of modes giving rise to strong, isolated, lines in the Raman spectrum, then, for these modes, the ratio A/B would depend only on the angle α. Considering a type II stacking, a relation can also be found between the angle δ between the molecules forming the herringbone and the ratio A/B, assuming weak intermolecular interactions. Here, the angular dependence of the intensities of the A_g crystal modes are still given by Eqn (6) if the monoclinic b-axis lies in the plane of the film. For weakly interacting molecules, the Raman tensors of some crystal modes of A_g (B_g) symmetry can be derived from those of A_{1g} molecular modes by making symmetric (antisymmetric) linear combinations of the molecular tensors rotated in relation to one another by an angle of $\pm\delta/2$ about the *molecular Y-axis*, similar to what is done in the oriented gas model.[42] This produces the required herringbone structure with its backbone (crystalline b-axis) contained in the plane of the film and leads to the relationship between the ratio A/B and the herringbone angle:

$$\sin^2(\delta/2) = (A/B+2)^{-1}\left[1-\left(\frac{\varepsilon}{1-\varepsilon}\right)(A/B)\right]. \tag{8}$$

Again, for modes with $\varepsilon \simeq 0$, the ratio A/B depends only on the structural parameter δ and should be the same for all Raman lines corresponding to such modes. Equation (8) is formally the same for δ and $180-\delta$; therefore, there are two possible solutions.

In both cases of Eqns (7) and (8), all such peaks in the spectra of samples with the same orientation and packing of molecules would yield similar values for A/B. However, if the intramolecular identity of the considered vibration is modified through strong intermolecular interactions, the value obtained for A/B for different peaks in a given spectrum need not bear a close relation with one another. Hence, the regularity of certain parameters obtained from fitting the angular dependence of the intensities of different peaks contains information about stacking and the strength of intermolecular interactions. The results of fitting the most intense peaks in the spectra with the expressions of Eqn (6) for different samples are listed in Table 3, and examples

Table 3. Ratio between the parameters A and B obtained by fitting with Eqn (6) the angular dependence of the intensities of selected Raman peaks in the P-polarisation. Lightly shaded areas designate suspected doublets while more heavy shading indicates confirmed ones (i.e. peaks to which the independent molecule approximations should not apply). ne. indicates *nonexistent* peaks

sample	S1	S3	S4	S5
ω (cm^{-1})		A/B		
583	—	3.92	5.60	15.50
733	2.17	4.79	4.87	7.83
836	1.90	ne.	ne.	ne.
930	1.89	ne.	ne.	ne.
966	ne.	—	9.25	—
1194	3.83	7.90	8.31	18.71
1316		7.02		23.81
1462		13.32		
1487		5.24		
1523		7.24		

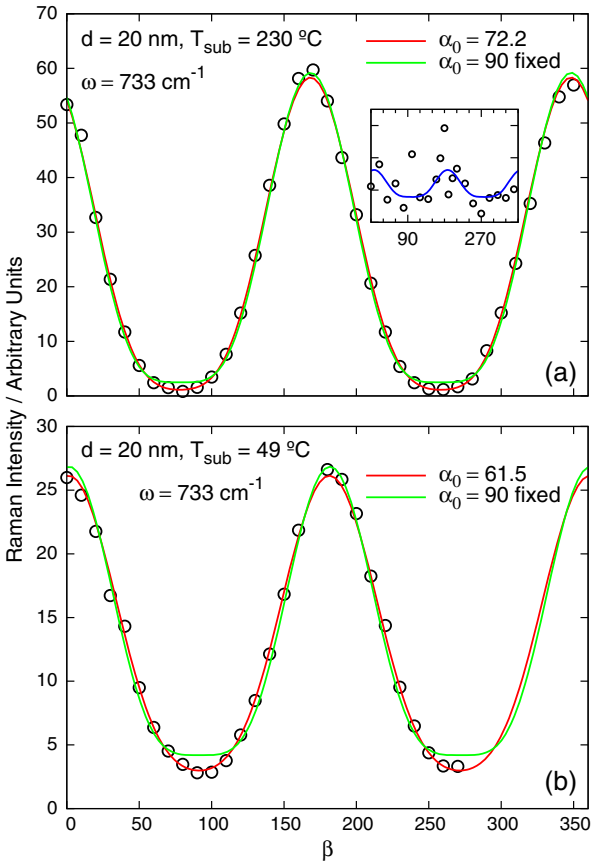

Figure 4. Angular dependence of the intensity of the peak a 733 cm^{-1} in the P-polarisation spectra of two samples of the same thickness grown on previously annealed A-plane sapphire at different substrate temperatures: (a) T_{subs} = 230 °C (S4) and (b) T_{subs} = 49 °C (S1). The inset shows the same dependence for a sample with little in-plane order (S2). The angles α_0 are values of α in degrees, see Eqn (7), obtained for this particular mode. The sensitivity of the azimuthal scans to the value α_0 is indicated by the lines. These data were partially shown in Fig. 7 of Ref. 22.

of the best fits obtained for parallel polarisations are shown in Fig. 4. Spectra in the P-configuration are about four times stronger than those of the C-configuration (see Table 2). Thus, the fittings obtained for the latter configurations (not shown) display a larger scatter in the experimental points. Hence, results for the C-configuration were mainly used to confirm the selection rules and to provide a comparison for the values of β_0 obtained in the fittings of the P-spectra. In all cases, good agreement was found between the fittings of both configurations, confirming that in these samples, in-plane ordering implies alignment (within two or three degrees) between the symmetry axis of the molecule or crystallite (or, rather, its projection on the plane of the film) and the *c*-axis of the sapphire substrate.

Comparing the values of A/B along a given row in Table 3 (same spectral feature for different samples), we observe marked differences. The values of this parameter for sample S1 (S5) are systematically lower (higher) than those for samples S3 or S4, which are very similar to one another. This points to a variation in the crystalline arrangements in the three kinds of samples. These results are consistent with weak intermolecular interactions (strong correlations between the values of *A*/*B* in a given sample) and different structural parameters (i.e. different values of α and δ) for samples grown at different conditions. Considering the two Raman peaks of frequencies 588 and 733 cm^{-1} in Figs. 2 (a) and 2(b) as examples of modes with $\varepsilon \simeq 0$, the average values of α obtained from these lines are: $\alpha \simeq (56 \pm 2)°, (65 \pm 2)°$, and $(73 \pm 4)°$ for samples S1, S3/S4, and S5, respectively. According to this, the molecules would be less inclined (more upright) in sample S5. This is in qualitative agreement with the different values of $d_\perp$ measured by X-ray diffraction.[22]

Evaluating the herringbone angle as $180 - \delta$ from Eqn (8) for the same Raman modes (as A_g modes originated from the A_{1g} modes), we obtain the values: $\delta \simeq (121 \pm 5)°, (135 \pm 6)°$, and $(143 \pm 6)°$ for samples S1, S3/S4, and S5, respectively. According to these results, the film deposited at lower temperature could be made up of crystallites of a phase isomorphic to γ-CuPc[13] whereas the structures of films deposited at higher temperature would present a herringbone packing tending to that obtained in a bulk F_{16}CuPc ribbon.[16] In this bulk structure, the molecules are shown with a slipped stacking which would be compatible with optical measurements.[19] The reported slipping distance is approximately 3.4 Å, and if we consider the measured interplanar distance[22] of $d_{||}$ = 32 Å, the molecular dipole dimers would form and angle of $\sim 43°$, which is sufficient to produce the observed[19] red shifted component[45] in the Q-band of these high-temperature films. Finally, regardless of the stacking type considered, we find the same result for the angle between the projection of the symmetry axis of the molecule (crystallite) and the c-axis of the sapphire substrate, β_0. Here $\beta_0 = 2.3 \pm 0.7°$ for all peaks of all samples in all frequency ranges.

The angular dependence of peak intensities can also be used to quantify the degree of order present in each sample. Totally disordered samples show no variations in peak intensity with

azimuthal angle. This can be appreciated by comparing the fit of the angular dependences of the intensity of the strongest peak in the spectrum of sample S5 [Fig. 4(a)] and that of sample S2 (inset of this figure). A quantitative idea of order can be obtained by adding a constant background, *C*, to the expressions of Eqn (6), as an additional fit parameter. An order parameter can be defined phenomenologically by comparing the value of this constant to that of the amplitude of modulation (A) in the following manner:

$$v = \frac{A^2}{A^2 + C} \tag{9}$$

The parameter v is thus very sensitive to any deviation of the mode angular dependence from a perfectly crystalline Raman tensor behaviour. The values of the order parameter thus obtained are listed in the last column of Table 1, which shows a steady decrease in order as the film thickness decreases (for samples deposited at the same temperature). This ranges from total order for the thickest sample (S5) to almost total disorder for the thinnest one (S2).

Now, we return to the discussion of the angular dependence of some of the components of the doublets at higher frequencies. We had pointed out before that, while the angular dependence of their intensities for the spectra with P-polarisation was qualitatively similar to those of the lower wavenumber peaks, the dependence for C-polarisation was qualitatively different [Fig. 2(d)], with maxima and minima located at different angular values. This behaviour is consistent with the existence of Davydov doublets in which the A_g members have intensities described by Eqn (6), while the B_g members would have intensities depending on rotation angle according to (Table 2):

$$I\left(x',x'\right) = e^2 \sin^2 2(\beta - \beta_0) + C, \qquad I\left(x',y'\right) = e^2 \cos^2 2(\beta - \beta_0) + C' \tag{10}$$

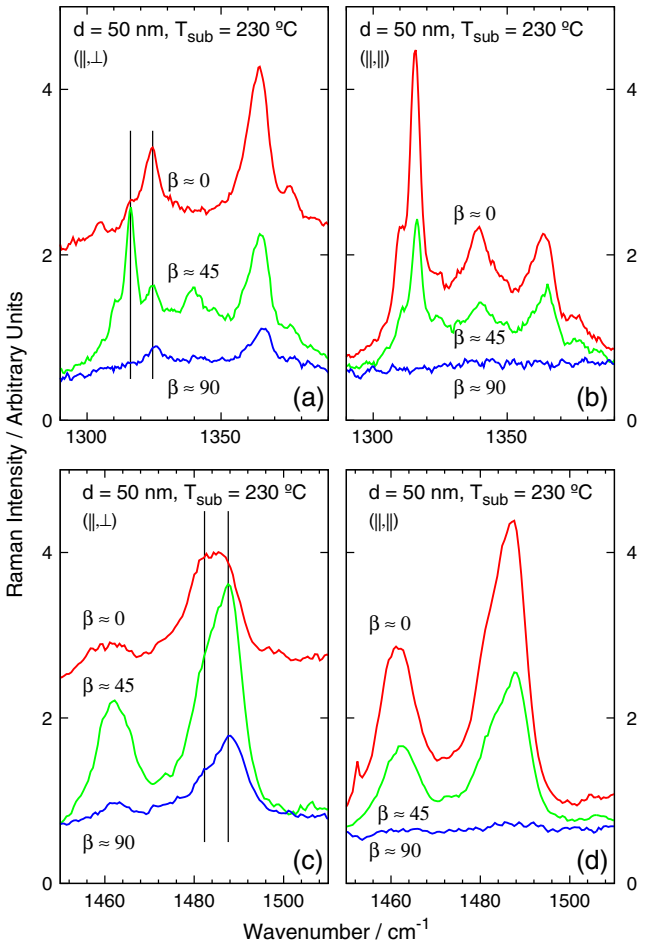

Figure 5. Detail of Davydov doublets in selected parts of the Raman spectrum of sample S5. The angular dependence of the intensities of different peaks is highlighted in order to display the A_g or B_g character.

Here, we have already assumed that the symmetry axis of the crystal lies in the plane of the film and a constant background (C,C′) has been added to the expressions of Table 2. The peaks in the high wavenumber parts of the Raman spectrum of sample S1 are wider and too close together to resolve the components of a given multiplet. Since sample S5 has the strongest signal and shows the highest degree of order, we concentrate on this sample. Note that the observation of these doublets is a qualitative signature of good crystalline quality. Figure 5 shows the relevant part of the Raman spectra of this sample, for both P and C polarisations. Parts (a) and (c) of this figure show structures that do not obey the description of Eqn (6), but are in qualitative agreement with that of Eqn (10). This suggests that these structures behave according to the B_g symmetry of the crystal. A quantitative comparison between the predictions of these equations and experimental data can at best be performed on the doublet indicated by vertical lines in Fig. 5(a) at 1316 and 1324 cm^{-1}, assigned to A_g and B_g symmetry, respectively. The measured splitting of 8 cm^{-1} is comparable to those observed in other molecular semiconductors.[23–26]

Next, we determine their intensities for different values of the angle β. This is not always easy, especially for the B_g member of the doublet, since the lines are very close together and have very different intensities, so noisy data and poor fits are expected. The results of this procedure are displayed as Supporting Information in Fig. S3(a) for P-polarisation and S3(b) for C-polarisation, respectively. In these figures, circles (triangles) denote experimental intensities for the A_g (B_g) member of the doublet while full and dotted lines represent fits with Eqns (6) and (10), respectively. In the upper part of the figure, the intensity of the B_g member of the doublet has been multiplied by a scaling factor of 10 in order to be able to represent both members of the doublet in the same figure. Since this peak is very weak and it rides on the much more intense A_g partner, this data is affected by very large uncertainties. In view of this, it is not surprising that the agreement between the data and the predictions of Eqn (10) for this peak is only qualitative. In spite of these difficulties, the angular dependence of the intensities of both peaks is well described by the equations corresponding to either A_g or B_g crystal symmetry. Quantitative agreement is best for the parallel polarisation line of the A_g member of the doublet (Fig. S3(a), circles and solid line). From the fit, parameters *A* and *B* are obtained. The *A*/*B* ratios obtained for this, and other high wavenumber A_g peaks of the samples S5 and S3, are also listed in Table 3.

The weakness of the B_g component of the doublets discussed above is probably a reflex of the weakness of the van der Waals intermolecular interactions within the film compared to intramolecular covalent bonding. However, the appearance of Davydov doublets with a B_g component is a direct consequence of the intermolecular interaction. As is clear from Table S2, each $A_g + B_g$

doublet derives from an intramolecular A_{1g} mode (A_g in site symmetry) as a result of the crystalline environment. For a weak interaction ratio practically the total Raman intensity will appear at the A_g component, as is the case here. The selection rules of the doublets are consistent with a film of monoclinic symmetry composed of herringbone molecular pairs. Strictly speaking, this result does not preclude a stacking of the first type, provided that molecules are not stacked in exact parallelism to one another. In either type I or II stacking, the *b*-axis of the resulting monoclinic structure would still be in the plane of the film. Other molecular arrangements might be possible, but it is difficult to imagine that they would produce the simple angular dependence of Raman intensities discussed here. Finally, the obtained Raman results are compatible and complementary to results from other techniques.

Conclusions

We have performed a systematic study of the Raman spectra of thin films of F_{16}CuPc deposited by OMBD on various substrates and under different growth conditions. Our analysis leads to interesting insights into the investigation of molecular stacking and in-plane order in these films. Of all the samples examined, only those deposited on previously annealed A-plane sapphire substrates show a high degree of in-plane order and have been presented in this report. This appears to be related to the presence of steps in the slightly miscut substrate surfaces that serve as templates for molecular orientation. However, in-plane order increases as the thickness of the deposited film increases, suggesting that the influence of the substrate on the growth is of comparable strength but smaller than the own crystal lattice energy.

Intermolecular interactions are thus relevant and are evident from the splittings of some vibration modes, particularly those involving motion of the more peripheral atoms. Davydov doublets are unequivocally identified in some high wavenumber vibrations by the Raman selection rules. In one particular cluster of peaks, a doublet is sufficiently well resolved to allow quantitative intensity *versus* β analysis of its $A_g - B_g$ components. However, the B_g/A_g intensity ratio is quite small suggesting that the intermolecular interactions are small compared to the intramolecular ones. The existence of doublets of these symmetries is consistent with the considered monoclinic crystal structure with two molecules per PC.

Uncoupled modes where the vibrating atoms are mainly those of the macrocycle inner ring largely retain the intramolecular character. We have related the Raman intensity angular variation of such modes to the orientation of molecules in the films. Although several molecular stackings could be compatible with the Raman data, two particular forms present the simplest picture which describes the observations. In one of them (type I), we consider single stacks of molecules arranged nearly parallel to one another. This allows a determination of the tilt angle between the planes of the molecule and the film surface, performed by fitting the observed dependence of the Raman intensities of selected spectral peaks, which yields angles of approximately 65° and 56° for films of comparable thickness deposited at 230 °C and 49 °C respectively. This indicates that at higher temperature the molecules attain on average a more upright configuration than at lower temperature. In the second, type II stacking, we consider that crystallites are formed having a herringbone structure with its axis parallel to the plane of the substrate. The analysis of the same uncoupled modes as crystalline modes which are obtained as linear combinations of the intramolecular vibrations allows to find a relationship leading to the apical angle δ of the herringbone. In this case, the derived angle between molecules is smaller for samples deposited at lower substrate temperature (resembling the γ polymorph of bulk CuPc crystals) and larger for those deposited at higher substrate temperature (more similar to the molecular packing described for bulk F_{16}CuPc ribbons). The performed analysis also provides quantitative estimates of the degree of in-plane order. In fact, some films are very well ordered, and therefore these spectra provide an improved reference for the Raman spectrum of F_{16}CuPc crystals.

Acknowledgements

This research has been partially funded by the Spanish Ministry of Science through grants MAT2009-10642 (Project NOMOCELL) and SAB1999-0195, a sabbatical stay of one of us (FC) at ICMAB which supported the start of this collaboration.

Supporting information

Supporting information may be found in the online version of this article.

References

[1] S. R. Forrest, *Chem. Rev.* **1997**, *97*, 1793.
[2] R. F. Bailey-Salzman, B. P. Rand, S. R. Forrest, *Appl. Phys. Lett.* **2007**, *91*, 013508.
[3] A. Opitz, J. Wagner, W. Brütting, A. Hinderhofer, F. Schreiber, *Phys. Status Solidi A* **2009**, *206*, 2683.
[4] K. Vasseur, B. P. Rand, D. Cheyns, L. Froyen, P. Heremans, *Chem. Mater.* **2011**, *23*, 886.
[5] F. Schreiber, *Phys. Status Solidi A* **2004**, *201*, 1037.
[6] T. Nyokong, in *Functional Phthalocyanine Molecular Materials*, vol. *135*, Springer Verlag, Heidelberg, **2010**, pp. 45–88.
[7] A. T. Davidson, *J. Chem. Phys.* **1982**, *77*, 168.
[8] C. G. Claessens, U. Hahn, T. Torres, *Chem. Rec.* **2008**, *8*, 75.
[9] Z. Bao, A. J. Lovinger, J. Brown, *J. Am. Chem. Soc.* **1998**, *120*, 207.
[10] X. H. Qiu, G. V. Nazin, W. Ho, *Phys. Rev. Lett.* **2004**, *92*, 206102.
[11] F.-C. Wu, H.-L. Cheng, C.-H. Yen, J.-W. Lin, S.-J. Liu, W.-Y. Chou, F.-C. Tang, *Phys. Chem. Chem. Phys.* **2010**, *12*, 2098.
[12] A. Troisi, *Chem. Soc. Rev.* **2011**, *40*, 2347.
[13] P. Erk, H. Hengelsberg, M. F. Haddow, R. van Gelder, *CrystEngComm* **2004**, *6*, 474.
[14] C. J. Brown, *J. Chem. Soc. A* **1968**, *1968*, 2488.
[15] Q. Tang, H. Li, Y. Liu, W. Hu, *J. Am. Chem. Soc.* **2006**, *128*, 14634.
[16] S. M. Yoon, H. J. Song, I.-C. Hwang, K. S. Kim, H. C. Choi, *Chem. Commun.* **2010**, *46*, 231.
[17] D. G. de Oteyza, E. Barrena, J. O. Ossó, S. Sellner, H. Dosch, *J. Am. Chem. Soc.* **2006**, *128*, 15052.
[18] F. Cerdeira, M. I. Alonso, M. Garriga, J. O. Ossó, V. Kruppa, F. Schreiber, H. Dosch, Proc. 26th Int. Conf. Phys. Semicond., Edinburgh 2002, IOP Conf. Series v. 171 CD-ROM, **2003**.
[19] M. I. Alonso, M. Garriga, J. O. Ossó, F. Schreiber, E. Barrena, H. Dosch, *J. Chem. Phys.* **2003**, *119*, 6335.
[20] J. O. Ossó, F. Schreiber, M. I. Alonso, M. Garriga, E. Barrena, H. Dosch, *Org. Electron.* **2004**, *5*, 135.
[21] E. Barrena, J. O. Ossó, F. Schreiber, M. Garriga, M. I. Alonso, H. Dosch, *J. Mater. Res.* **2004**, *19*, 2061.
[22] J. O. Ossó, F. Schreiber, V. Kruppa, H. Dosch, M. Garriga, M. I. Alonso, F. Cerdeira, *Adv. Funct. Mater.* **2002**, *12*, 455.
[23] M. Loi, Q. Cai, H. Chandrasekhar, M. Chandrasekhar, W. Graupner, G. Bongiovanni, A. Mura, C. Botta, F. Garnier, *Synth. Met.* **2001**, *116*, 321.
[24] A. Degli Esposti, M. Fanti, M. Muccini, C. Taliani, G. Ruani, *J. Chem. Phys.* **2000**, *112*, 5957.

[25] D. A. Tenne, S. Park, T. U. Kampen, A. Das, R. Scholz, D. R. T. Zahn, *Phys. Rev. B* **2000**, *61*, 14564.
[26] T. Jentzsch, H. Juepner, K.-W. Brzezinka, A. Lau, *Thin Solid Films* **1998**, *315*, 273.
[27] C. A. Melendres, V. A. Maroni, *J. Raman Spectrosc.* **1984**, *15*, 319.
[28] C. Jennings, R. Aroca, A. Hor, R. O. Loutfy, *J. Raman Spectrosc.* **1984**, *15*, 34.
[29] A. J. Bovill, A. A. McConnell, J. A. Nimmo, W. E. Smith, *J. Phys. Chem.* **1986**, *90*, 596.
[30] D. Christen, V. Hoffmann, A. Rager, W. Göpel, *Thin Solid Films* **1992**, *208*, 284.
[31] B. A. Kolesov, T. V. Basova, I. K. Igumenov, *Thin Solid Films* **1997**, *304*, 166.
[32] T. V. Basova, B. A. Kolesov, *Thin Solid Films* **1998**, *325*, 140.
[33] D. R. Tackley, G. Dent, W. Ewen Smith, *Phys. Chem. Chem. Phys.* **2001**, *3*, 1419.
[34] T. V. Basova, V. G. Kiselev, B.-E. Schuster, H. Peisert, T. Chassé, *J. Raman Spectrosc.* **2009**, *40*, 2080.
[35] G. H. Watson, W. B. Daniels, C. S. Wang, *J. Appl. Phys.* **1981**, *52*, 956.
[36] M. J. Frisch, G. W. Trucks, H. B. Schlegel, G. E. Scuseria, M. A. Robb, J. R. Cheeseman, V. G. Zakrzewski, J. A. Montgomery, Jr., R. E. Stratmann, J. C. Burant, S. Dapprich, J. M. Millam, A. D. Daniels, K. N. Kudin, M. C. Strain, O. Farkas, J. Tomasi, V. Barone, M. Cossi, R. Cammi, B. Mennucci, C. Pomelli, C. Adamo, S. Clifford, J. Ochterski, G. A. Petersson, P. Y. Ayala, Q. Cui, K. Morokuma, D. K. Malick, A. D. Rabuck, K. Raghavachari, J. B. Foresman, J. Cioslowski, J. V. Ortiz, A. G. Baboul, B. B. Stefanov, G. Liu, A. Liashenko, P. Piskorz, I. Komaromi, R. Gomperts, R. L. Martin, D. J. Fox, T. Keith, M. A. Al-Laham, C. Y. Peng, A. Nanayakkara, C. Gonzalez, M. Challacombe, P. M. W. Gill, B. G. Johnson, W. Chen, M. W. Wong, J. L. Andres, M. Head-Gordon, E. S. Replogle, J. A. Pople. *Gaussian 98, Revision A.7*, Gaussian, Inc., Pittsburgh, PA, **1998**.
[37] C. J. Brown, *J. Chem. Soc. A* **1968**, *1968*, 2494.
[38] J. R. Ferraro, K. Nakamoto, C. W. Brown, *Introductory Raman Spectroscopy* (2nd edn), Academic Press, San Diego, **2003**.
[39] W. G. Fateley, N. T. McDevitt, F. F. Bentley, *Appl. Spectrosc.* **1971**, *25*, 155.
[40] E. Burgos, H. Bonadeo, E. D'Allesio, *J. Chem. Phys.* **1975**, *63*, 38.
[41] A. Brillante, I. Bilotti, R. G. Della Valle, E. Venuti, A. Girlando, *CrystEngComm* **2008**, *10*, 937.
[42] G. C. Pimentel, A. L. McClellan, W. B. Person, O. Schnepp, *J. Chem. Phys.* **1955**, *23*, 234.
[43] R. Scholz, A. Y. Kobitski, T. U. Kampen, M. Schreiber, D. R. T. Zahn, G. Jungnickel, M. Elstner, M. Sternberg, T. Frauenheim, *Phys. Rev. B* **2000**, *61*, 13659.
[44] R. Scholz, L. Gisslén, B.-E. Schuster, M. B. Casu, T. Chassé, U. Heinemeyer, F. Schreiber, *J. Chem. Phys.* **2011**, *134*, 014504.
[45] M. Kasha, H. R. Rawls, M. A. El-Bayoumi, *Pure Appl. Chem.* **1965**, *11*, 371.